FIBERGLASS COMPOSITE REINFORCEMENT WITH NANOCELLULOSE FIBER SIZING

Ejaz Haque, Joyanta Goswami, Robert J. Moon, Douglas M. Fox, Kyriaki Kalaitzidou

Georgia Institute of Technology
813 Ferst Dr. NW
Atlanta, GA 30332

ABSTRACT

Domestic automotive production has been undergoing a decades-long shift toward lightweight materials that aims to yield substantial economic and environmental benefits. In this time, research advances have been made that could theoretically enable industrial-scale production of composites that are even lighter than what currently dominates the market. However, these newer materials fail to strike the balance between weight, performance, and cost necessary to disrupt the status quo. One pathway to overcoming this challenge lies in the use of nanomaterial additives that are capable of enhancing overall composite properties without significantly impacting weight or cost. Nanocellulose is a promising nanomaterial for this application, as it exhibits a high strength to weight ratio and, as a plant-based biomaterial, can be produced abundantly and renewably. The goal of this work is to enhance fiber-matrix adhesion in fiberglass composites by incorporating nanocellulose on the glass fiber surface. In doing so, the mechanical properties of these composites are improved, establishing a theoretically scalable pathway toward reductions in glass fiber loading and, consequently, composite weight. Chemical and mechanical characterization shows that nanocellulose does indeed enhance the interface, and this effect can be tuned through adjustment of nanocellulose surface chemistry.

1. INTRODUCTION

Industrial focus on lightweight materials in automotive production has been developing over the last several decades as a result of shifting market trends and government policy. Advances in composites technologies during that time have enabled manufacturers to substitute increasing quantities of traditional metals with lighter composite replacements each year. Though this trend is expected to experience further growth in the coming years, this can only occur if lightweight components develop in such a way that they can replace larger, performance-critical sections of the vehicle design. Doing so requires that these new materials maintain a balance of weight, cost, and performance to disrupt the automotive materials market.

One approach to addressing this issue is using nanofillers to enhance composite properties or reduce their weight. Nanoclay platelets, for example, have been incorporated into nylon-6 for enhanced toughness in under the hood applications [1]. For weight reduction applications, cellulose nanocrystals (CNC) are a promising reinforcing agent due to their high performance and environmental compatibility associated with the abundance and renewability of their plant-based sources [2]. Incorporation of CNC into polymer composites has previously proven effective in

SAMPE Conference Proceedings. Charlotte, NC, May 20-23, 2019. Society for the Advancement of Material and Process Engineering – North America.

improving mechanical properties such as tensile and flexural strength and moduli [3]. However, these approaches involving direct mixing of the nanofiller into the polymer matrix are often challenging due to limited processing scalability associated with efficient nanofiller exfoliation and use of solvent.

This work describes a method for improving glass fiber-epoxy composite properties through novel fiber coatings. By circumventing the need to incorporate the nanofiller into the matrix, this approach offers a potentially scalable pathway toward composite weight reduction. These fiber coatings contained CNC of different surface functionalities to understand their roles in fiber-matrix interfacial interactions and optimize mechanical property improvement.

2. EXPERIMENTATION

2.1 Materials

ME1510 multiend rovings (TEX 4800, 10 μm diameter) purchased from Owens Corning (Oak Brook, IL, USA) were the glass fibers used in this series of experiments. An epoxy system comprising US Composites (West Palm Beach, FL, USA) 635 thin epoxy and 556 slow amine hardener was used as the polymer matrix. 99 % diiodomethane, a probe liquid used in surface energy assessment, was also purchased from Sigma Aldrich.

Two types of CNC were used in this study: a relatively common variety sulfuric acid-hydrolyzed CNC (CNC-S) manufactured by the Forest Products Laboratory and purchased through the University of Maine (Orono, ME, USA), and a CNC modified with methyl(triphenyl) phosphonium functionality (CNC-Ph) provided by the laboratory of Douglas M. Fox at American University (Washington D.C., USA). CNC-S also acts as the starting material for the modification that produces CNC-Ph, and this modification is intended to provide a steric effect that minimizes CNC self-aggregation, thereby retaining the inherently high mechanical properties of individual nanocellulose crystals [4]. CNC-S were reported to be between 5-20 nm in width and 150-200 nm in length according to University of Maine specifications, and the dimensions of CNC-Ph were found to fall within a similar range [4].

2.2 Solution Preparation and Fiber Coating

The coating formulations described in Table 1 were chosen to analyze the effects of CNC surface functionality on various interfacial characteristics. All solutions were prepared using a combination of magnetic stirring and sonication to mix and dilute the as-received CNC, as well as to break up aggregated particles. Single glass fibers were then mounted on a metal frame and dip coated in the sonicated solutions for 5 minutes. Fibers were dried in ambient conditions overnight and reserved for various analyses.

Table 1. Coating formulations and their respective shorthand notation.

Coating Label	Coating Composition
GF0	N/A – as-received
GF1	CNC-S 1 %
GF2	CNC-Ph 1 %

2.3 Single Fiber Fragmentation Testing

Dried single glass fibers were mounted in a dogbone-shaped mold using polyimide tape to maintain tension. A 2:1 mixture of the epoxy resin and amine hardener was stirred magnetically for 3 minutes, degassed in a vacuum chamber for 5 minutes, then poured over the dried fibers and cured for 1 hour at 100 ºC followed by 2 hours at 120 ºC. The cured epoxy coupons were then subjected to single fiber fragmentation testing (SFFT), in which an Instron 33R 4466 was used to apply tensile load to the coupons along the fiber direction (ASTM D638). The test was run at a crosshead displacement rate of 1 mm/min for 3 to 5 minutes.

Depending on the type of coating applied to the fiber prior to curing, it was necessary to adjust the testing duration to ensure that fracture saturation was achieved. Saturation is defined as the point in testing at which the maximum number of fiber fractures (areas where the fiber breaks due to its axial stress reaching its tensile strength) is attained. As the fiber continues to break as a result of shear forces from the applied load, the distance between fracture points along the fiber will become so small that the load transferred across the matrix will be unable to exceed the fiber's tensile strength, and fracturing will thus cease. This saturation point was determined by making SFFT coupons for each coating and monitoring fracture count after tensile testing. These calibration tests were concluded once predetermined strain limits were reached. Once no additional fragmentation was observed upon increasing this limit, this point was used as the saturation point for that coating.

The number of fiber fragments in each sample was determined using polarized light optical microscopy. The number of fragments can be used to assess the load transfer efficiency and by comparing between different samples the effects of fiber coating formulations can be compared directly.

2.4 Microscopic Characterization

Microscopic characterization was used to assess the coatings on the glass fibers, as well as the fracture events at the glass fiber-polymer interface within SFFT samples after testing. Coating morphology on the fiber surface was observed using a Phenom G2 Pro scanning electron microscope (SEM) to image coated fibers. For SFFT samples, the fragment length (i.e., distance between breaks), quantity of fiber fragments, and geometry of fracture patterns were all observed using a Leica DM2500 polarized light optical microscope. The same microscope was used to observe the coating morphology of the silicon wafers described in the next section.

2.5 Spin Coating and Contact Angle Analysis

Due to its impact on film formation and coating uniformity on the fiber surface, surface energy was assessed for the CNC solutions. Calculations were performed using sessile drop shape analysis on silicon wafers spin coated in the coating formulations of interest. Droplets of distilled water and diiodomethane were placed on these coated wafers, and their contact angles were measured using a Ramé-Hart Model 250 goniometer. These values were in turn used to determine the surface energy of the coatings using the Fowkes' surface energy theory, an extension of Young's Equation that described surface energy by its polar and dispersive components [5]:

$$(\sigma_S^D)^{1/2} * (\sigma_L^D)^{1/2} + (\sigma_S^P)^{1/2} * (\sigma_L^P)^{1/2} = \frac{\sigma_L(\cos\theta + 1)}{2} \quad [1]$$

$$\sigma_S^D = \frac{\sigma_L(\cos\theta + 1)^2}{4} \quad [2]$$

σ_S represents the unknown surface energy of the coating film and σ_L represents the known surface energy of the probe liquid. The superscripts represent corresponding dispersive and polar components. σ_S^D can be determined through measurement of contact angle θ with diiodomethane since the σ_L^P for diiodomethane is 0 and σ_L^D is thus equivalent to σ_L. In this case, Equation 1 reduces to Equation 2, which can be used to solve for σ_S^D. σ_S^D can then be used in Equation 1 alongside the surface energy components of water to determine σ_S^P, which is then added to σ_S^D to yield the total solid surface energy for a given film.

3. RESULTS

The results presented herein focus on select representative data regarding the effect of CNC functionality on various interfacial characteristics. Investigation into the impact of other coating factors has also been conducted, and once analysis is completed, the results of those experiments may be presented alongside the current work at a later time.

3.1 Interfacial Mechanical Properties

The results from SFFT are shown in Figure 1. All coated fibers yielded higher average fragment counts than the as-received fiber GF0 with a sample size of 5 to 7 dogbones. The average values were highest in the case of GF2-coated fibers, though this improvement was not quite high enough to exhibit statistical significance at a 99% confidence interval.

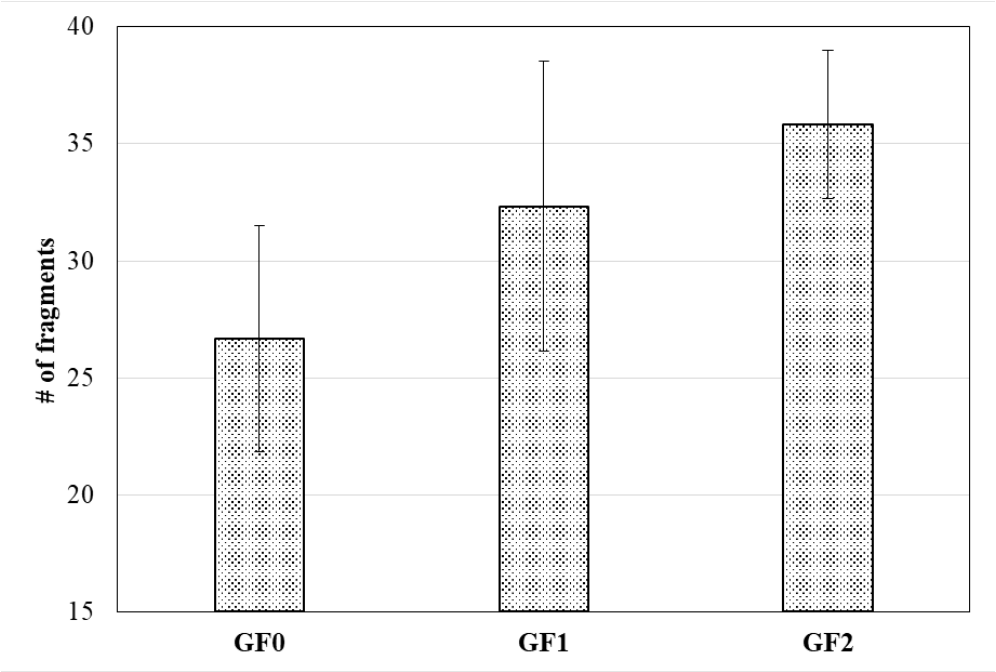

Figure 1. Fiber fragment count after SFFT for as-received fibers (GF0), CNC-S coated fibers (GF1), and CNC-Ph coated fibers (GF2). Error bars are one standard deviation.

3.2 SFFT Fracture Mode

In addition to fragment count, fracture geometry was also monitored using polarized light optical microscopy. Type 1 is a thin, disk-shaped matrix crack perpendicular to the fiber indicative of a strong interface, Type 2 is a double-cone shaped crack indicative of a moderately strong interface, and Type 3 is a thin perpendicular crack surrounded by a long birefringence pattern indicative of matrix debonding and a weak interface.

The effect of CNC functionality on fracture mode is shown in Figure 2. GF0, the fiber with the lowest average fragment count as shown in Figure 1, exhibited exclusively Type 3 fractures with long, dark debonding patterns surrounding the fracture area (Fig. 2a). GF1 also exhibited primarily Type 3 fractures (Fig. 2b), however the length of these patterns was noticeably shorter on average than in the case of GF0, indicating some minor improvement in the strength of the interface. GF2 yielded further improvements, displaying both Type 2 and Type 3 fractures along the fiber length (Fig. 2c). This observation expands upon the results from Figure 1 and suggests that CNC-Ph improves fiber-matrix adhesion to a greater extent than CNC-S.

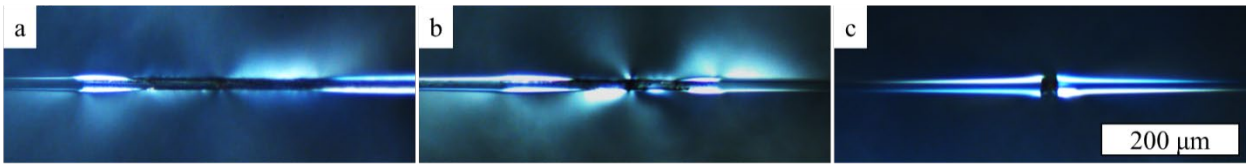

Figure 2. Fiber fracture modes, indicative of interface strength, observed for: a) as-received fibers (GF0), b) CNC-S coated fibers (GF1), and c) CNC-Ph coated fibers (GF2).

3.3 Coating Morphology

Coated and dried fibers were observed via SEM and the results are shown in Figure 3. GF0, the as-received fiber, exhibited thin streaks of pre-existing sizing from the manufacturer that could also be seen in the thin coatings of GF1 and GF2. Darker, non-homogeneous patches could be seen across the length of the fiber, indicative of interaction between CNC and the fiber surface. This in turn affects the topography of the fiber surface, and the increased surface roughness may explain the observed increase in fragmentation due to its effect on energy absorption [6].

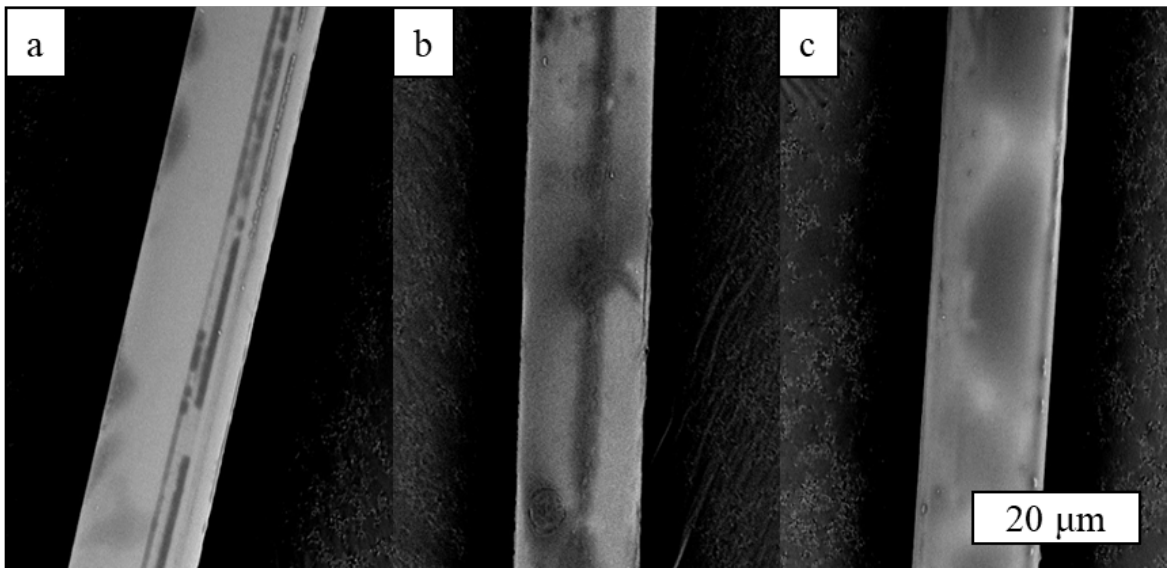

Figure 3. Fiber surfaces analyzed via SEM for: a) as-received fibers (GF0), b) CNC-S coated fibers (GF1), and c) CNC-Ph coated fibers (GF2).

Differences in coating uniformity were further studied through microscopy of silicon wafers spin coated in the solutions of interest. The flat surfaces of the wafers enabled a clearer understanding of the impact of CNC functionality on spreading behavior, as shown in Figure 4. Both types of CNC uniformly adjusted the transmittance color of the silicon wafer from a light grey to a light orange. Additionally, aggregated crystals of varying sizes could be seen across the surface of the wafer. Rough estimates of aggregate size were made using a Profilm3D optical profilometer, which revealed that the height of these aggregates ranged from approximately 0.5 to 3.3 µm. These observations served to support the claim that CNC were indeed present on the fiber surfaces shown in Figure 3, as well as the notion that CNC coatings can be distributed somewhat uniformly across the fiber surface. The latter observation supports the increases in fragmentation shown in Figure 1, as uniform film formation is among the most impactful variables in determining interfacial adhesion [7].

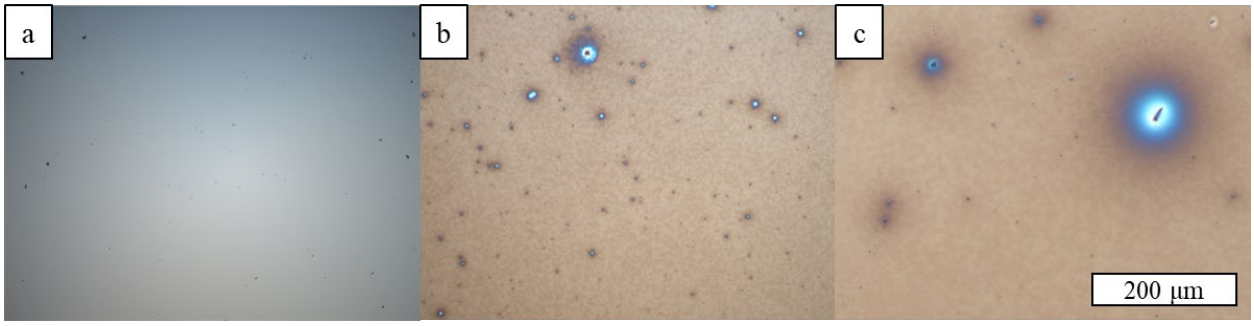

Figure 4. Silicon wafers spin coated in: a) no coating, b) CNC-S, and c) CNC-Ph.

3.4 Surface Energy

The impact of CNC on spreadability was quantified through surface energy analysis. The polar and dispersive components of the surface energy for CNC coatings are shown in Table 2. A moderate polar:dispersive ratio was calculated for these samples, as expected due to the surface groups present on the CNC. As glass is itself a moderately polar material, this may explain the increased affinity for the fiber surface exhibited by solutions containing CNC. However, substantiating this conclusion would require imaging and spectroscopic techniques such as energy dispersive x-ray spectroscopy or x-ray photoelectron spectroscopy.

Table 2. Calculated surface energy values for spin coated CNC formulations.

Coating	σ_S^D (mN/m)	σ_S^P (mN/m)	σ_S (mN/m)
GF1	47.4	30.0	77.4
GF2	48.2	29.2	77.4

4. CONCLUSIONS

CNC with multiple surface functionalities were applied to the surface of glass fibers. Application of these CNC resulted in enhancement of the fiber-matrix interphase in epoxy composites beyond what the pre-existing sizing offers. It was found that CNC with a surface modification intended to minimize aggregation (CNC-Ph) provided the greatest average improvement in interfacial properties. Optical microscopy corroborated the observation that the performance of CNC-Ph is greater than that of the more common CNC-S. CNC were also shown to provide relatively homogenous coatings on silicon wafer surfaces, but more studies would need to be done to quantify this phenomenon.

The authors would like to thank P^3 Nano and the U.S. Endowment for Forestry and Communities for funding this work, as well as Owens Corning and Michelman Inc. for providing the glass fibers and commercial sizing formulation. Special acknowledgement is given to Dr. Jeffrey W. Gilman and Dr. Gale A. Holmes for their insights with regards to testing protocol and data interpretation.

5. REFERENCES

1. Naskar, A.K., J.K. Keum, and R.G. Boeman, *Polymer matrix nanocomposites for automotive structural components.* Nature nanotechnology, 2016. **11**(12): p. 1026.
2. Moon, R.J., et al., *Cellulose nanomaterials review: structure, properties and nanocomposites.* Chemical Society Reviews, 2011. **40**(7): p. 3941-3994.
3. Asadi, A., et al., *Introducing cellulose nanocrystals in sheet molding compounds (SMC).* Composites Part A: Applied Science and Manufacturing, 2016. **88**: p. 206-215.
4. Fox, D.M., et al., *Simultaneously tailoring surface energies and thermal stabilities of cellulose nanocrystals using ion exchange: effects on polymer composite properties for transportation, infrastructure, and renewable energy applications.* ACS applied materials & interfaces, 2016. **8**(40): p. 27270-27281.
5. Fowkes, F.M., *Attractive forces at interfaces.* Industrial & Engineering Chemistry, 1964. **56**(12): p. 40-52.

6. Gao, X., et al., *Effect of colloidal silica on the strength and energy absorption of glass fiber/epoxy interphases.* Composites Part A: Applied Science and Manufacturing, 2011. **42**(11): p. 1738-1747.
7. Mäder, E., E. Moos, and J. Karger-Kocsis, *Role of film formers in glass fibre reinforced polypropylene—new insights and relation to mechanical properties.* Composites Part A: Applied Science and Manufacturing, 2001. **32**(5): p. 631-639.